Ring-shaped quantum droplets with hidden vorticity in a radially periodic potential

Bin Liu [1,2] Xiaoyan Cai,[1] Xizhou Qin,[1,2] Xunda Jiang,[1,2] Jianing Xie,[1,2,*] Boris A. Malomed [3,4] and Yongyao Li [1,2]

[1]*School of Physics and Optoelectronic Engineering, Foshan University, Foshan 528000, China*
[2]*Guangdong-Hong Kong-Macao Joint Laboratory for Intelligent Micro-Nano Optoelectronic Technology,*
Foshan University, Foshan 528000, China
[3]*Department of Physical Electronics, School of Electrical Engineering, Faculty of Engineering,*
and Center for Light-Matter Interaction, Tel Aviv University, Tel Aviv 69978, Israel
[4]*Instituto de Alta Investigación, Universidad de Tarapacá, Casilla 7D, Arica, Chile*

We study the stability and characteristics of two-dimensional circular quantum droplets (QDs) with embedded hidden vorticity (HV), i.e., opposite angular momenta in two components, formed by binary Bose-Einstein condensates (BECs) trapped in a radially periodic potential. The system is modeled by the Gross-Pitaevskii equations with the Lee-Huang-Yang terms, which represent the higher-order self-repulsion induced by quantum fluctuations around the mean-field state, and a potential which is a periodic function of the radial coordinate. Ring-shaped QDs with high winding numbers (WNs) of the HV type, which are trapped in particular circular troughs of the radial potential, are produced by means of the imaginary-time-integration method. Effects of the depth and period of the potential on these QD states are studied. The trapping capacity of individual circular troughs is identified. Stable compound states in the form of nested multiring patterns are constructed too, including ones with WNs of opposite signs. The stably coexisting ring-shaped QDs with different WNs can be used for the design of BEC-based data-storage schemes.

I. INTRODUCTION

Bose-Einstein condensates (BECs) have long been an ideal platform for studying various physical problems, such as stability and dynamics of self-localized states [1–6]. It is well known that the cubic self-attraction gives rise to stable bright solitons only in effectively one-dimensional (1D) systems. The natural sign of the mean-field (MF) nonlinearity for a BEC is self-repulsive, while it may be switched into attraction, which is necessary for self-trapping of solitons, by means of the Feshbach resonance [7] . However, in two-dimensional (2D) and three-dimensional (3D) settings, matter-wave solitons are destabilized by the occurrence of the critical and supercritical collapses, respectively, in the same dimension [8–10]. Therefore, stabilization of multidimensional solitons, especially vorticity-carrying ones, is a well-known challenging problem [11]. The most common method for the solution of the problem is to modify the nonlinearity. This is possible with the help of quadratic self-interaction [12], competitive self-focusing and defocusing terms [13–16], saturable self-attraction [17], and nonlocal nonlinearity [18–22]. Other methods use spin-orbit coupling in binary BECs [23–26], the harmonic-oscillator trapping potential [27,28], or spatially periodic (lattice) potentials [29].

Recently, a kind of quantum matter, in the form of quantum droplets (QDs), has been experimentally created in dipolar [30,31] and binary bosonic gases [32]. QDs rely on their intrinsic nonlinearity to form stable self-localized states.

The formation of QDs was predicted based on the balance between the MF self-attraction and the repulsion induced by quantum fluctuations beyond the MF approximation [33,34]. The latter effect is represented by the Lee-Huang-Yang (LHY) [35] corrections added to the corresponding Gross-Pitaevskii (GP) equations. The predictions demonstrate that the LHY terms take different forms in 1D, 2D, and 3D systems, being self-repulsive in the 2D and 3D cases. Studies of QDs have drawn much interest in very different contexts [36–69]. Stable QDs with embedded vorticity have been predicted in 2D and 3D forms [70,71], including semidiscrete vortex QDs in arrays of coupled 1D matter-wave conduits [72] . However, stability conditions for vortex QDs become increasingly stricter with the increase of their winding number (WN, alias the topological charge). Therefore, searching for experimentally relevant settings that promote the existence of such stable topological modes is a relevant problem. QDs in an effectively 1D system have been considered too, where the quadratic LHY term added to the GP equation is self-attractive, on the contrary to its sign in the 3D and 2D settings [73–75].

Another possibility for the stabilization of nonlinear vortex modes has been revealed by studies of BEC systems under the action of spatially periodic and quasiperiodic lattice potentials [76–85]. It has been predicted that periodic potentials not only help to stabilize self-bound vortex modes but also alter their formation dynamics. The same pertains to localized states with *hidden vorticity* (HV), which are defined as two-component states with equal norms and opposite angular momenta (i.e., opposite vorticities) of their components [86]. HV states in BECs in a rotating double-well potential were considered in Refs. [87,88].

---

*xiejianingfs@126.com

044210-1

As an experimentally relevant means of supporting stable self-trapped vortex modes, especially ones with high topological charges, it is more natural to use radial potential which, unlike the spatially periodic ones, conserve the angular momentum. In Ref. [89], authors reported stable vortex solitons with WN $S = 11$ maintained by the radial potential in a dipolar BEC with repulsive long-range dipole-dipole interactions, and in Ref. [90], authors reported stable narrow vortex-ring QDs with high values of S trapped in particular circular troughs of the radial potential. Further, in Ref. [90], authors reported stable compound states in the form of multiple mutually nested concentric rings. However, such complexes are stable only when the inner and outer annular components of the nested complexes are widely separated; hence, they practically do not interact.

The objective of this paper is to demonstrate that stable 2D ring-shaped QDs of the HV type can be created and controlled in binary BECs with contact interactions, using radially periodic potentials. The dynamics of the system are modeled by coupled GP equations including the LHY terms and radial-periodic potential. The corresponding annular (ring-shaped) HV QDs are trapped in particular circular troughs of the radial potential. The effects of the modulation depth and period of the potential states are systematically studied. Throughout this investigation, stability areas are identified vs the number of the trapping radial trough and WN of the HV states. Then nested complexes of annular QDs that carry different WNs are addressed. The results offer the possibility to design an encoding device that makes use of coexisting HV ring-shaped QDs with different WNs for storing data components.

The rest of the paper is structured as follows. The model is introduced in Sec. II, numerical findings and some analytical estimates regarding 2D ring-shaped HV QDs are summarized in Sec. III, and multiring nested patterns with different WNs in concentric circular troughs are the focus of Sec. IV. This paper is concluded by Sec. V.

II. THE MODEL

Following Refs. [91,92], we assume that QDs, which are formed by binary BEC, are relatively loosely confined in the transverse direction z, with confinement size $a_\perp \sim$ a few microns, relative to the plane of the system (x, y). The corresponding system of coupled GP equations for wave functions $\Psi_{1,2}$ of two components of the binary condensate, including the LHY correction (quartic self-repulsion) can be written as

$$i\hbar \frac{\partial}{\partial t}\Psi_j = \left(-\frac{\hbar^2}{2m}\nabla^2_{3D} + V(\mathbf{r}) + \frac{\delta E_{\text{total}}}{\delta n_j}\right)\Psi_j, \quad (1)$$

$$E_{\text{total}} = E_{\text{MF}} + E_{\text{LHY}}, \quad (2)$$

where $j = 1, 2$, $\nabla^2_{3D} = \partial^2_z + \nabla^2_{2D}$, and $\nabla^2_{2D} \equiv \partial^2_r + r^{-1}\partial_r + r^{-2}\partial^2_\theta$ is the 2D Laplacian written in the polar coordinates, while $V(\mathbf{r})$ is the potential. The total energy includes the MF and LHY terms:

$$E_{\text{MF}} = \int_{-\infty}^{+\infty} dz \int_0^\infty r\, dr \int_0^{2\pi} d\theta$$
$$\times \left(\frac{1}{2}g_{11}n_1^2 + g_{12}n_1n_2 + \frac{1}{2}g_{22}n_2^2\right), \quad (3)$$

$$E_{\text{LHY}} = \frac{8m^{3/2}}{15\pi^2\hbar^3} \int_{-\infty}^{+\infty} dz \int_0^\infty r\, dr \int_0^{2\pi} d\theta$$
$$\times (g_{11}n_1 + g_{22}n_2)^{5/2}, \quad (4)$$

where $n_j = |\Psi_j|^2$ are the densities, g_{11}, g_{22}, and g_{12} are strengths of the MF self- and cross-interactions of the two species, which satisfy constraints $g_{11}, g_{22} > 0$ and $g_{12} + \sqrt{g_{11}g_{22}} < 0$ [33]. Here, we consider the case of equal masses, i.e., $m_1 = m_2 = m$, and $g_{i,j} = 4\pi a_{i,j}/m$, where $a_{11,12}$ and a_{12} are the intraspecies and interspecies scattering length, respectively. It is well known that Feshbach resonances are an important tool for extracting information about interactions between atoms. In addition, they provide a way to change the scattering length almost at will [93]. If we consider, as usual, the symmetric system, with $g = g_{11} = g_{22} > 0$ and $g_{12} = -(g + \delta g)$, with $\delta g > 0$, the system of the GP equations is obtained in the form of

$$i\hbar \frac{\partial \Psi_1}{\partial t} = -\frac{\hbar^2}{2m}\nabla^2_{3D}\Psi_1 + g(|\Psi_1|^2 - |\Psi_2|^2)\Psi_1$$
$$- \delta g|\Psi_2|^2\Psi_1 + \frac{4g^{5/2}m^{3/2}}{3\pi^2\hbar^3}$$
$$\times (|\Psi_1|^2 + |\Psi_2|^2)^{3/2}\Psi_1 + V(\mathbf{r})\Psi_1,$$

$$i\hbar \frac{\partial \Psi_2}{\partial t} = -\frac{\hbar^2}{2m}\nabla^2_{3D}\Psi_2 + g(|\Psi_2|^2 - |\Psi_1|^2)\Psi_2$$
$$- \delta g|\Psi_1|^2\Psi_2 + \frac{4g^{5/2}m^{3/2}}{3\pi^2\hbar^3}$$
$$\times (|\Psi_1|^2 + |\Psi_2|^2)^{3/2}\Psi_2 + V(\mathbf{r})\Psi_2. \quad (5)$$

Adopting, as said above, the potential $V(\mathbf{r})$ as

$$V(\mathbf{r}) = V(x, y) + \frac{1}{2}m\omega_z^2 z^2, \quad (6)$$

one can carry out the 3D → 2D reduction by substituting

$$\Psi_{1,2}(x, y, z, t) = \Phi_{1,2}(x, y, t)\left(\frac{m\omega_z}{\pi\hbar}\right)^{1/4}$$
$$\times \exp\left(-\frac{m\omega_z}{2\hbar}z^2 - i\frac{\omega_z}{2}t\right) \quad (7)$$

into Eq. (5) and averaging the equations in the z direction, which yields

$$i\hbar \frac{\partial \Phi_1}{\partial t} = -\frac{\hbar^2}{2m}\nabla^2_{2D}\Phi_1 + \left(\frac{m\omega_z}{3\pi\hbar}\right)^{1/2}$$
$$\times [g(|\Phi_1|^2 - |\Phi_2|^2) - \delta g|\Phi_2|^2]\Phi_1$$
$$+ \left(\frac{m\omega_z}{\pi\hbar}\right)^{3/4}\frac{2g^{5/2}m^{3/2}}{3\pi^2\hbar^3}$$
$$\times (|\Phi_1|^2 + |\Phi_2|^2)^{3/2}\Phi_1 + V(x, y)\Phi_1,$$

$$i\hbar \frac{\partial \Phi_2}{\partial t} = -\frac{\hbar^2}{2m}\nabla^2_{2D}\Phi_2 + \left(\frac{m\omega_z}{3\pi\hbar}\right)^{1/2}$$
$$\times [g(|\Phi_2|^2 - |\Phi_1|^2) - \delta g|\Phi_1|^2]\Phi_2$$
$$+ \left(\frac{m\omega_z}{\pi\hbar}\right)^{3/4}\frac{2g^{5/2}m^{3/2}}{3\pi^2\hbar^3}$$
$$\times (|\Phi_1|^2 + |\Phi_2|^2)^{3/2}\Phi_2 + V(x, y)\Phi_2. \quad (8)$$

Furthermore, the radially periodic potential is taken as [94]

$$
V(x, y) = \frac{\hbar^2 k_r^2}{2m} \cos^2\left(\frac{\pi}{D_0} r\right),
$$

$$
k_r = \frac{2\pi}{\lambda}, \quad r = \sqrt{x^2 + y^2}, \tag{9}
$$

where D_0 is the radial period of the potential, and λ is the laser wavelength of potential building. Such a potential can be readily imposed by a broad laser beam passed through a properly designed phase plate [95]. By means of rescaling with length unit r_0 and following transformations:

$$
t' = \frac{\hbar}{mr_0^2} t, \quad x' = x/r_0, \quad y' = y/r_0,
$$

$$
D = D_0/r_0, \quad \psi_{1,2} = r_0 \Phi_{1,2},
$$

$$
V(x', y') = \frac{mr_0^2}{\hbar^2} V(x, y),
$$

$$
g' = \frac{m}{\hbar^2}\left(\frac{m\omega_z}{3\pi\hbar}\right)^{1/2} g,
$$

$$
\delta g' = \frac{m}{\hbar^2}\left(\frac{m\omega_z}{3\pi\hbar}\right)^{1/2} \delta g,
$$

$$
\Gamma = \frac{m}{r_0\hbar^2} \frac{2g^{5/2}m^{3/2}}{3\pi^2\hbar^3}\left(\frac{m\omega_z}{\pi\hbar}\right)^{3/4}, \tag{10}
$$

Eq. (8) is cast in the normalized form:

$$
i\frac{\partial\psi_1}{\partial t} = -\frac{1}{2}\nabla_{2D}^2\psi_1 + g(|\psi_1|^2 - |\psi_2|^2)\psi_1
$$

$$
- \delta g|\psi_2|^2\psi_1 + \Gamma(|\psi_1|^2 + |\psi_2|^2)^{3/2}\psi_1
$$

$$
+ V_0\cos^2\left(\frac{\pi}{D}r\right)\psi_1,
$$

$$
i\frac{\partial\psi_2}{\partial t} = -\frac{1}{2}\nabla_{2D}^2\psi_2 + g(|\psi_2|^2 - |\psi_1|^2)\psi_2
$$

$$
- \delta g|\psi_1|^2\psi_2 + \Gamma(|\psi_1|^2 + |\psi_2|^2)^{3/2}\psi_2
$$

$$
+ V_0\cos^2\left(\frac{\pi}{D}r\right)\psi_2, \tag{11}
$$

where V_0 and D are the accordingly rescaled depth and radial period of the potential. Localized solutions of Eq. (11) are characterized by their 2D norm:

$$
N_{2D} = \int_0^\infty r\,dr \int_0^{2\pi} d\theta(|\psi_1|^2 + |\psi_2|^2). \tag{12}
$$

According to the Refs. [93–95], the nonlinear coefficient and LHY corrections can be adjusted by Feshbach resonances, and the wavelength and incident angle of the laser are also adjusted. In this paper, we refer to parameters for BECs of ^{39}K atoms, the potential-building laser wavelength $\lambda = 1064$ nm, transverse-confining frequency $\omega_z = 2\pi \times 200$ Hz, and rescaling length $r_0 = 0.08\lambda$, which yields $g = 0.057$, $\delta g = g/10$, and $\Gamma = 0.0049$. A typical simulation time, for which the results are reported below, $t = 20\,000$, is equivalent to ≈ 100 ms in physical units, which is a sufficiently large time for the experiment. While according to Eqs. (7) and (12), the total atoms are N_{2D}.

The objective of this paper is to predict stable ring-shaped QDs of the HV type as solutions of Eq. (11). They are defined by fixing WNs and chemical potentials of the two components as $S_2 = -S_1 = -S$ and $\mu_2 = \mu_1 = \mu$ [86]. Thus, we seek stationary HV solutions in the form of

$$
\psi_1(r, \theta, t) = \phi_1(r)\exp(-i\mu t + iS\theta),
$$

$$
\psi_2(r, \theta, t) = \phi_2(r)\exp(-i\mu t - iS\theta), \tag{13}
$$

where real functions $\phi_{1,2}$ obey radial equations:

$$
\mu\phi_1 = -\frac{1}{2}\left(\frac{d^2}{dr^2} + \frac{1}{r}\frac{d}{dr} - \frac{S^2}{r^2}\right)\phi_1
$$

$$
+ g(|\phi_1|^2 - |\phi_2|^2)\phi_1 - \delta g|\phi_2|^2\phi_1
$$

$$
+ \Gamma(|\phi_1|^2 + |\phi_2|^2)^{3/2}\phi_1 + V_0\cos^2\left(\frac{\pi}{D}r\right)\phi_1,
$$

$$
\mu\phi_2 = -\frac{1}{2}\left(\frac{d^2}{dr^2} + \frac{1}{r}\frac{d}{dr} - \frac{S^2}{r^2}\right)\phi_2
$$

$$
+ g(|\phi_2|^2 - |\phi_1|^2)\phi_2 - \delta g|\phi_1|^2\phi_2
$$

$$
+ \Gamma(|\phi_2|^2 + |\phi_1|^2)^{3/2}\phi_2 + V_0\cos^2\left(\frac{\pi}{D}r\right)\phi_2. \tag{14}
$$

Stationary ring-shaped QD vortices trapped in radial potential troughs with numbers $O_n = 1, 2, 3\ldots$ can be produced by means of the imaginary-time-propagation (ITP) method [96,97]. It was applied to Eq. (11) with the Gaussian initial guess:

$$
\psi_{10}(r, \theta) = C_1\exp[-\alpha_1(r - r_n)^2 + iS\theta],
$$

$$
\psi_{20}(r, \theta) = C_2\exp[-\alpha_2(r - r_n)^2 - iS\theta], \tag{15}
$$

where $\alpha_{1,2} > 0$ and $C_{1,2}$ are real constants, and

$$
r_n = \left(O_n - \frac{1}{2}\right)D \tag{16}
$$

is the radial coordinate of the bottom point of the given trough. Then the stability of the stationary ring-shaped QDs was analyzed by means of the linearized Bogoliubov–de Gennes (BdG) equations for perturbed wave functions:

$$
\psi_1(x, y, t) = [\phi_1(x, y) + \varepsilon w_1(x, y)\exp(\lambda t + im\theta)
$$

$$
+ \varepsilon v_1^*(x, y)\exp(\lambda^* t - im\theta)]
$$

$$
\times \exp(-i\mu t + iS\theta),
$$

$$
\psi_2(x, y, t) = [\phi_2(x, y) + \varepsilon w_2(x, y)\exp(\lambda t - im\theta)
$$

$$
+ \varepsilon v_2^*(x, y)\exp(\lambda^* t + im\theta)]
$$

$$
\times \exp(-i\mu t - iS\theta), \tag{17}
$$

where $w_{1,2}(x, y)$, $v_{1,2}(x, y)$, and λ are eigenmodes, instability growth rate corresponds to an integer azimuthal index m of the perturbation with infinitesimal amplitude ε, and $*$ stands for the complex conjugate. The substitution of the ansatz in Eq. (17) into Eq. (11) and linearization leads to the following system of the BdG equations:

$$
\begin{pmatrix} A_{11} & A_{12} & A_{13} & A_{14} \\ A_{21} & A_{22} & A_{23} & A_{24} \\ A_{31} & A_{32} & A_{33} & A_{34} \\ A_{41} & A_{42} & A_{43} & A_{44} \end{pmatrix}\begin{pmatrix} w_1 \\ v_1 \\ w_2 \\ v_2 \end{pmatrix} = i\lambda\begin{pmatrix} w_1 \\ v_1 \\ w_2 \\ v_2 \end{pmatrix}, \tag{18}
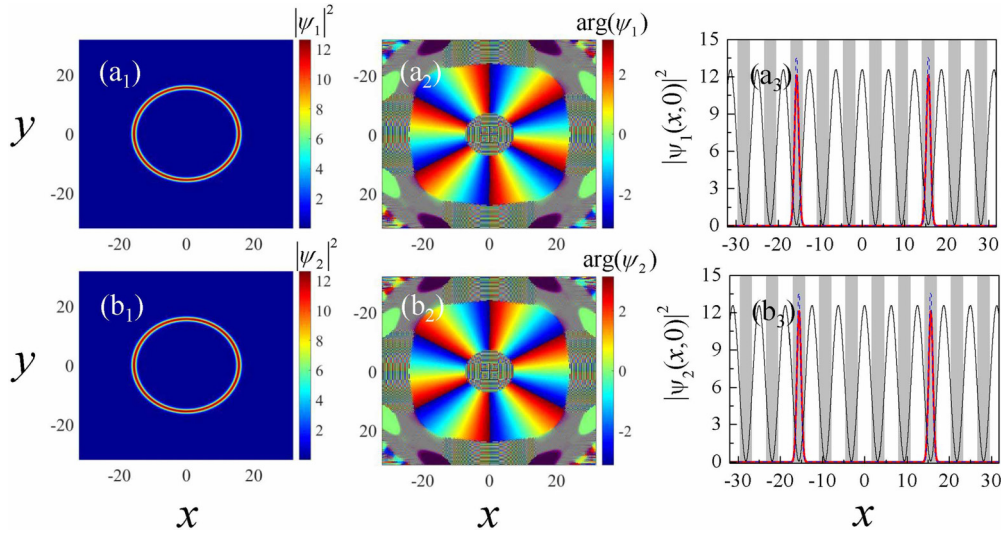$$

FIG. 1. Typical examples of stable ring-shaped quantum droplets (QDs) of the hidden vorticity (HV) type trapped in the trough with $O_n = 3$. (a_1) and (b_1) Density patterns of the two components with $N = 3000$, $V_0 = 12.63$, and $S_{1,2} = \pm 6$. (a_2) and (b_2) The corresponding phase patterns. The red curves in (a_3) and (b_3) correspond to the cross-section $|\psi_{1,2}(x,0)|^2$, along $y = 0$, in (a_1) and (b_1). Here, the blue dashed lines represent, for the sake of comparison, the result for $V_0 = 18.95$; other parameters remain the same. The black lines represent the axisymmetric radially periodic potential with depth $V_0 = 12.63$ and period $D = 6.25$.

with matrix elements $A_{11} \sim A_{44}$ given in the Appendix.

Numerically solving the linearized equations produces a spectrum of eigenfrequencies λ, the stability condition being that the entire spectrum of λ must be pure imaginary [98,99]. The so-predicted stability of the stationary states was then verified by direct simulations of the perturbed evolution, using the fast-Fourier-transform method.

III. SINGLE-RING STATES

Stationary ring-shaped QDs of the HV type, trapped in radial potential troughs with $O_n = 1, 2, 3$, and 4, were produced by means of the ITP method. Typical examples of a numerically constructed QDs with $S_{1,2} = \pm 6$, which are trapped in the trough with $O_n = 3$, are displayed in Figs. 1(a_1) and 1(b_1). This situation corresponds to the largest WN $|S_1| = |S_2|$ that admits stability for $O_n = 3$, as shown below in Fig. 5(c). HV phase patterns are shown in Figs. 1(a_2) and 1(b_2), which confirm the condition $S_2 = -S_1$. The density cross-sections $|\psi_{1,2}(x,0)|^2$, which are displayed in Figs. 1(a_3) and 1(b_3), corroborate the placement of the QDs in the third potential trough. Here, the norm is $N = 3000$, and the radial period and depth of the potential in Eq. (11) are $D = 6.25$ and $V_0 = 12.63$, respectively. While the inner radius of HV QDs in the 2D free space increases with the increase of the WN and total norm, the radius of the HV QDs trapped the radially periodic potential stays nearly constant, being determined by r_n, see Eq. (16).

The stability of the ring-shaped HV QDs was verified by direct simulations of the perturbed evolution and also through eigenvalues produced by the BdG Eq. (18) for small perturbations. Figure 2 shows typical examples of stable and unstable QDs with WNs $S_{1,2} = \pm 2$ trapped in the potential trough with $O_n = 2$, for different values of the total norm N. Here, we present direct simulations and the perturbation eigenvalues with different azimuthal indices m, see Eq. (17).

Figure 2(a_1) shows direct simulations of the ψ_1 component of a stable ring-shaped HV QD with 1% random noise, and $N = 1500$. Further, Fig. 2(b_1) shows the same for an unstable HV QD, here $N = 150$. The latter result may be interpreted as fragmentation of the original azimuthally uniform state as a result of its modulational instability. Further, Figs. 2(a_2) and 2(b_2) show the perturbation eigenvalues for the corresponding
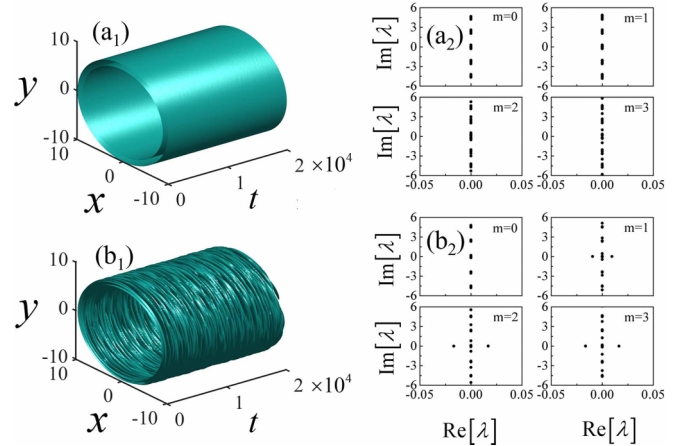

FIG. 2. (a_1) Direct simulations of the ψ_1 component of a stable hidden vorticity (HV) quantum droplet (QD) with $S_{1,2} = \pm 2$ and $N = 1500$. (a_2) Perturbation eigenvalues for the same mode, for azimuthal indices $m = 0, 1, 2$, and 3. (b_1) The same as in (a_1) but for an unstable mode with $N = 150$. (b_2) Perturbation eigenvalues for this mode, with azimuthal indices $m = 0, 1, 2$, and 3. The ring-shaped modes displayed in this figure are trapped in the potential trough with $O_n = 2$, other parameters being the same as in Fig. 1. Here, 1% random noise is added with initial ansatz $\psi_{1,2}(x, y, t = 0) = [1 + \varepsilon' f(x, y)] \cdot \phi_{1,2}(x, y)$, where $\varepsilon' = 1\%$ and $f(x, y)$ is a random function with the value range $[0, 1]$ that can be generated by the rand function.
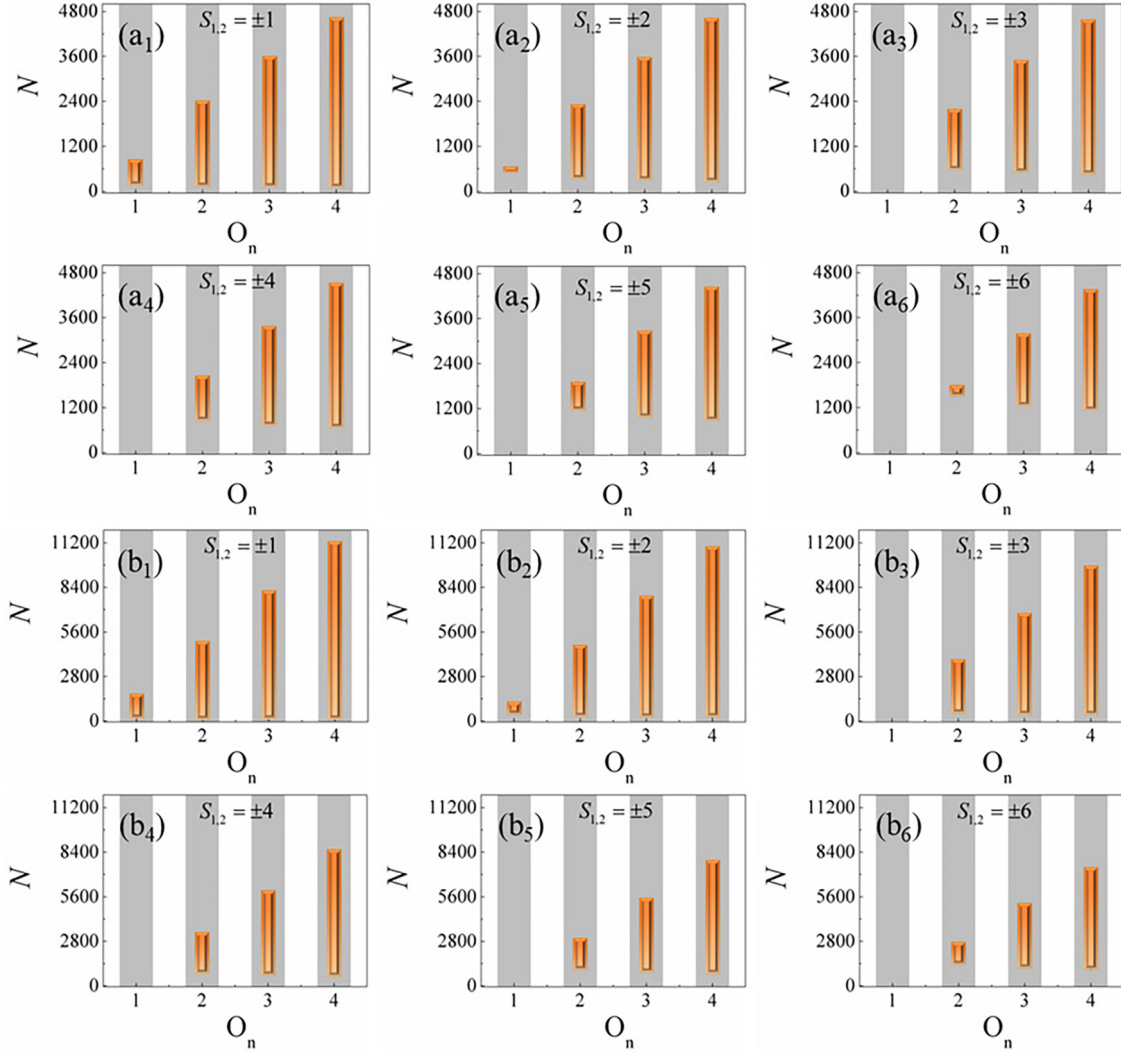
FIG. 3. (a_1)–(a_6) and (b_1)–(b_6) Orange bars represent stability intervals for hidden vorticity (HV) ring-shaped quantum droplets (QDs) with $S_{1,2} = \pm 1$, ± 2, ± 3, ± 4, ± 5, and ± 6, respectively, trapped in radial-potential troughs with numbers $O_n = 1, 2, 3$, and 4. The depth of the potential is $V_0 = 12.63$ in (a_1)–(a_6) and $V_0 = 18.95$ in (b_1)–(b_6). The radial period is $D = 6.25$.

modes with $N = 1500$ and 150, respectively, for azimuthal indices $m = 0, 1, 2$, and 3. The results of direct simulations are consistent with the prediction of the linear-stability analysis.

The results of the numerical analysis of the stability of the HV ring-shaped QDs with different WNs are summarized in Fig. 3 for different values of the potential depth, viz., $V_0 = 12.63$ and 18.95 [Figs. 3(a_1)–3(a_6) and 3(b_1)–3(b_6), respectively] and the period of the radial potential $D = 6.25$. In this figure, stability areas are represented by orange bars in the plane of (N, O_n). It is seen that, for fixed values of $|S_{1,2}|$ and V_0, the HV QDs are stable in finite intervals, i.e., $N_{\min} < N < N_{\max}$. At $N < N_{\min}$, such modes do not exist, while at $N > N_{\max}$, they spill out into the next radial trough or multiple troughs.

The fact that the length of the stability interval in Fig. 3 increases with the increase of O_n can be explained as follows. The densities in the different O_n are comparable; then the total norm will be larger for higher n due to the increase in the size of the potential from the radial geometry. The peak-density

difference of the HV QDs in the stability region is

$$\triangle I = I_T - I_B, \tag{19}$$

where I_T and I_B (represented by the red and black dotted lines, respectively, in Fig. 4) are values of the peak density at the top and bottom of the orange bars. The green bars in Fig. 4 illustrate the peak density of the stable HV ring-shaped QDs with $S_{1,2} = \pm 1$ trapped at $O_n = 1, 2, 3$, and 4, with $V_0 = 12.63$ in (a) and $V_0 = 18.95$ in (b). The numerical results yield $\triangle I_1 \approx 14.09$ and $\triangle I_2 \approx 31.29$ in Figs. 4(a) and 4(b), respectively. Different from ring-shaped QDs with explicit, rather than hidden, vorticity trapped in radially periodic potentials [90], the peak-density difference $\triangle I$ of the present modes substantially increases with the increase in V_0.

Further, comparing the above results for $V_0 = 12.63$ [Figs. 3(a_1)–3(a_6)] and $V_0 = 18.95$ [Figs. 3(b_1)–3(b_6)], we conclude that the stability intervals are shorter in the former case. This finding can be explained too. The increase in the depth of the potential V_0 causes a slight decrease of the radial
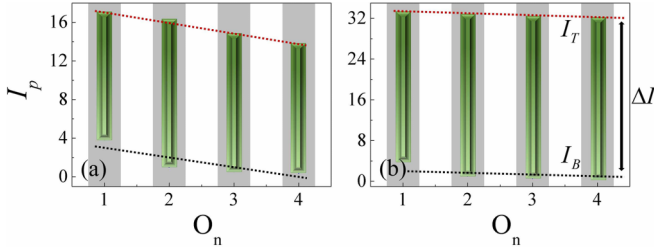
FIG. 4. The peak density of the stable hidden vorticity (HV) ring-shaped quantum droplets (QDs) with $S_{1,2} = \pm 1$, trapped in the radial troughs with $O_n = 1, 2, 3,$ and 4. The parameters are $D = 6.25$ in both panels, and $V_0 = 12.63$ in (a) or $V_0 = 18.95$ in (b). The numerical results yield $\Delta I_1 = I_T - I_B \approx 14.09$ in (a) and $\Delta I_2 = I_T - I_B \approx 31.29$ in (b).

width w of the HV QDs, as can be seen from the cross-section of $|\psi(x,0)|^2$ in Fig. 1(a$_3$), where the red and blue dashed curves correspond to $V_0 = 12.63$ and 18.95, respectively. However, as said above, the peak density difference ΔI is larger in the latter case. According to Ref. [90], this results in increase of ΔN. It is also worth noting that, as is shown by the comparison with Ref. [90], the size of the stability intervals of the HV states is smaller than their counterparts with the explicit vorticity, for equal values of the norm and WNs.

The dependence of the chemical potential μ of the HV QDs on the total norm N is plotted in Fig. 5(a), where parameters are the same as in Fig. 3(a$_2$). The $\mu(N)$ curves feature a positive slope $d\mu/dN > 0$, violating the well-known Vakhitov-Kolokolov (VK) criterion, which is a necessary stability condition for self-trapped modes maintained by a self-attractive nonlinearity [10,11,99]. In Fig. 5(a), the solid and dotted lines represent values of μ of stable and unstable HV ring-shaped QDs, respectively. On the other hand, for localized modes supported by self-repulsive nonlinearity (such as gap soliton), the necessary stability condition is the opposite, given by the anti-VK criterion $d\mu/dN > 0$ [100].

In the case of the competition between the self-attraction and repulsion in Eq. (11), it is not *a priori* obvious which condition, VK or anti-VK, is a dominant one for the stability. To resolve the issue, we first employ a straightforward estimate for the peak density of the ring-shaped modes:

$$I_p \approx \frac{N}{\pi(2O_n - 1)Dw},\qquad(20)$$

where w is the effective width of the HV QDs in the radial direction. Next, following Ref. [90], we apply the Thomas-Fermi (TF) approximation to Eq. (14), dropping the second-derivative terms in it, which yields

$$\mu_{\rm TF} = -\delta g I_p + 2\sqrt{2}\Gamma I_p^{3/2} + \tfrac{1}{2}V_0.\qquad(21)$$

By combining this expression with Eq. (20), we conclude that $d\mu/dN > 0$ takes place above a threshold value:

$$N > N_{\rm th} = \frac{\pi(2O_n - 1)Dw(\delta g)}{18\Gamma^2}.\qquad(22)$$

In our computations, the radial period is fixed as $D = 6.25$, and if we select $w = D/2$, then the $N_{\rm th}$ values in Eq. (22) for $O_n = 1, 2, 3, 4,$ and 5 are $N_{\rm th} \approx 4.59, 13.77, 22.94, 32.12,$
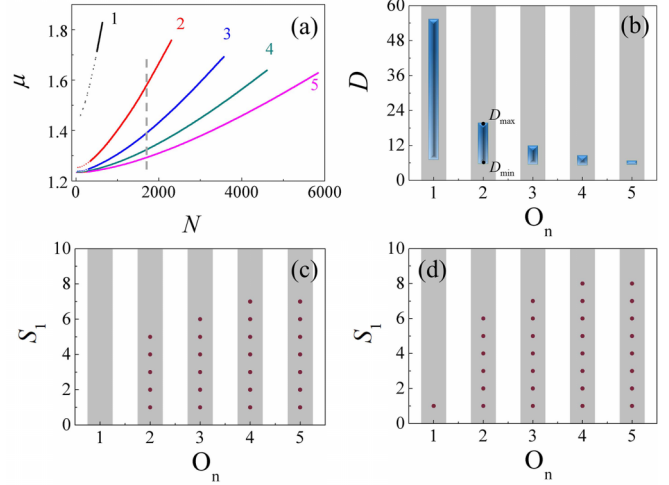

FIG. 5. (a) The dependence of the chemical potential μ on norm N for hidden vorticity (HV) ring-shaped quantum droplets (QDs) with $S_{1,2} = \pm 2$, where the parameters are the same as in Fig. 3(a$_2$). Solid and dotted segments represent stable and unstable QDs, respectively. The vertical dashed line illustrates the coexistence of stable modes with equal norms which are trapped in the troughs with different numbers O_n. (b) Boundary values ($D_{\min}$ and $D_{\max}$) of the period of the radial potential for given values of O_n, between which the HV ring-shaped QDs are stable, the other parameters being $N = 1500$, $V_0 = 12.63$, and $S_{1,2} = \pm 2$. Trapping ability of the radial-potential troughs for HV ring-shaped QDs with indicated values of winding numbers (WNs) $|S_{1,2}|$ in the radial troughs with numbers O_n and (c) $V_0 = 12.63$ or (d) $V_0 = 18.95$, the other parameters being $N = 1500$ and $D = 6.25$.

and 41.3, respectively. On the other hand, it is seen in Fig. 5(a) that numerically found bottom stability boundaries for $O_n = 1, 2, 3, 4,$ and 5 are $N_{\min} \approx 508, 343, 304, 282,$ and 262, respectively, which are all much larger than $N_{\rm th}$ for each value of O_n; hence, the anti-VK criterion indeed determines the stability in this case.

The multistability of the HV ring-shaped QDs, which may coexist as stable modes with the same norm, trapped in the troughs with different numbers O_n, is illustrated by the vertical dashed line in Fig. 5(a). In this case, it is relevant to compare energies of the coexisting modes. The Hamiltonian density corresponding to Eq. (11) is

$$\mathcal{H} = \frac{1}{2}(|\nabla\psi_1|^2 + |\nabla\psi_2|^2) + \frac{g}{2}(|\psi_1|^4 + |\psi_2|^4)$$
$$- (g + \delta g)|\psi_1|^2|\psi_2|^2 + \frac{2\Gamma}{5}(|\psi_1|^2 + |\psi_2|^2)^{5/2}$$
$$+ V_0\cos^2\left(\frac{\pi}{D}r\right)(|\psi_1|^2 + |\psi_2|^2).\qquad(23)$$

Using Eq. (23), one can find that, among the HV QDs with equal norms and equal values of $|S_{1,2}|$, the minimum energy $\iint \mathcal{H}dxdy$ corresponds to the number O_n of the largest ring.

The effect of the period of the radial potential D on the HV QDs is presented in Fig. 5(b), where the other parameters are fixed as $N = 1500$, $S_{1,2} = \pm 2$, and $V_0 = 12.63$. Our results demonstrate that the modes are stable in certain intervals
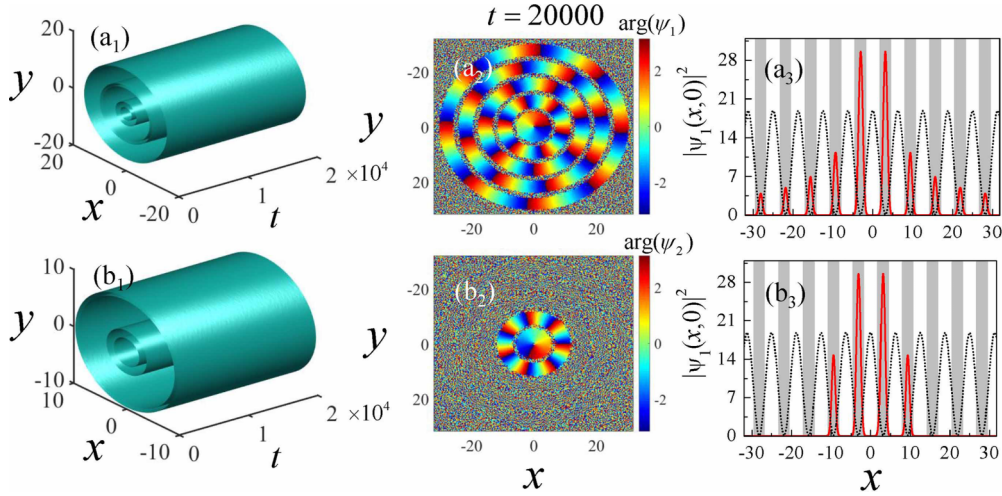
FIG. 6. Typical examples of stable multiring (nested) hidden vorticity (HV) quantum droplets (QDs). (a_1) Direct simulations of the evolution of the ψ_1 component for a stable multiring state with parameters $(N, S_{1,2}, O_n) = (1500, \pm1, 1)$, $(1500, \pm6, 2)$, $(1500, \pm7, 3)$, $(1500, \pm8, 4)$, and $(1500, \pm8, 5)$. (a_2) The output phase pattern of the same state at $t = 20\,000$. (a_3) The cross-section along $y = 0$, $|\psi_{1,2}(x, 0)|^2$, plotted by the red curves. (b_1) Direct simulations of the evolution of the ψ_1 component for a stable two-ring HV mode with opposite signs of $S_{1,2}$ in the rings, with parameters $(N, S_{1,2}, O_n) = (1500, \pm1, 1)$ and $(2000, \mp7, 2)$. (b_2) The output phase pattern of the same mode at $t = 20\,000$. (b_3) The cross-section along $y = 0$, $|\psi_{1,2}(x, 0)|^2$, plotted by red curves. Other parameters are the same as in Fig. 5(d).

$D_{min} < D < D_{max}$ for given ring numbers O_n, viz.,

$$\Delta D \equiv D_{max} - D_{min} \propto \frac{1}{(2O_n - 1)}. \qquad (24)$$

This finding may be explained, in terms of the above-mentioned modulational instability, by attenuation of the stabilizing effect of the curvature of the ring, which scales as $(2O_n - 1)^{-1}$.

With the norm fixed to $N = 1500$ and the radial period fixed to $D = 6.25$, the ability of the radial potential in Eq. (9) to maintain the stable HV ring-shaped QDs with high values of WN, $|S_{1,2}|$, at different numbers of O_n is illustrated in Figs. 5(c) and 5(d) for $V_0 = 12.63$ and 18.95, respectively. The results are consistent with those presented in Figs. 3(a_1) and 3(b_1). For $V_0 = 12.63$, no stable solutions are found at $O_n = 1$, which is explained by the fact that the above-mentioned value $N_{max} = 838$ is smaller than the fixed norm adopted here $N = 1500$, for $S_{1,2} = \pm1$ at $O_n = 1$. On the other hand, the HV ring-shaped QDs with $S_{1,2} = \pm1$ at $O_n = 1$ are found for $V_0 = 18.95$ because, in that case, we have $N_{min} = 153 < 1500 < N_{max} = 1695$. In Figs. 5(c) and 5(d), one can see that the holding capacity of the radial troughs increases with the increase of O_n, and these plots also reveal that the increase of the depth of the potential naturally enhances the capacity of the trough to hold stable HV QDs.

IV. NESTED HV QDS

Nested structures are stable concentric states in which self-trapped vortex rings carrying different WNs (topological charges) are embedded into each other. This concept was introduced for dissipative ring-vortex solitons [101]. Later, nested multiring states with different WNs trapped in different radial troughs were produced [90]. The results of those studies demonstrate that mutually embedded ring-shaped vortical

may be stable if the separation between the rings is large enough.

Typical examples of stable concentric HV states are displayed in Fig. 6, where panel (a_1) shows the result of direct simulations for the ψ_1 component, which is composed of five concentric HV QDs with $(N, S_{1,2}, O_n) = (1500, \pm1, 1)$, $(1500, \pm6, 2)$, $(1500, \pm7, 3)$, $(1500, \pm8, 4)$, and $(1500, \pm8, 5)$. This mode stays stable during time exceeding 100 ms in physical units. Its phase pattern at $t = 20\,000$ is shown in Fig. 6(a_2), and the density cross-section $|\psi_1(x, 0)|^2$ is displayed in Fig. 6(a_3).

It is worth considering the case of nested states composed of ring-shaped HV QDs with opposite signs of WNs. A typical example of a stable concentric mode of this type, with parameters of $(N, S_{1,2}, O_n) = (1500, \pm1, 1)$ and $(2000, \mp7, 2)$, is displayed in Fig. 6(b_1). Additionally, the output phase pattern and density cross-section $|\psi_1(x, 0)|^2$ are displayed in Figs. 6(b_2) and 6(b_3).

In this paper, the radially periodic potential can maintain self-trapping of HV ring-shaped QDs in particular troughs. If the QDs are stable in their troughs, the corresponding nested patterns are also stable, the reason being that the HV rings trapped in different troughs are nearly isolated from each other. These results offer a potential use in the design of data-storage devices, in which different data components, coded by the respective WN values, may be deposited in different radial troughs.

V. CONCLUSIONS

The purpose of this paper is to establish stability and characteristics of 2D ring-shaped QDs with HV formed by binary BECs in the radially periodic potential. The system is modeled by the coupled GP equations with the LHY terms,

which represent the correction to the MF theory produced by quantum fluctuations, and the radial potential. Families of ring-shaped QDs with the HV structure, represented by high values of the WN, trapped in particular circular troughs of the radial potential, have been produced. Effects of the depth and period of the radial potential on the ring-shaped HV QDs were studied, and their stability area was identified. It was found that the size of the stability interval increases with the increase of the trough number O_n. On the other hand, the stability interval naturally expands with the increase of the depth of the potential. For stable HV ring-shaped QDs, the dependence between the chemical potential and total norm obeys the anti-VK criterion, which is explained by the dominant role of the self-repulsive LHY nonlinearity. The multistability of the HV states was demonstrated, in the form of the coexistence of the modes with equal norms and WNs but different radii of the trapping circular trough. The trapping capacity of the troughs was identified for the HV ring-shaped QDs with different WNs. Nested patterns composed of rings with different WNs, trapped in different radial troughs, were constructed, including two-ring patterns with opposite WN signs. The results reported in this paper suggest a alternative approach to the creation of stable nested QDs with embedded WNs. These results may also be used in the design of data-storage devices, with stable WN rings trapped in different radial troughs encoding data components.

The analysis can be extended in other directions—one can consider ring-shaped QDs of the HV type in an elliptically deformed potential. A challenging possibility is to the extend the consideration for 3D settings.

APPENDIX

The matrix elements $A_{11} \sim A_{44}$ in the linearized BdG Eq. (18) are

$$A_{11} = -\frac{1}{2}\left[\frac{d}{rdr} + \frac{d^2}{dr^2} - \frac{(S+m)^2}{r^2}\right] + \left[2g|\phi_1|^2 - (g+\delta g)|\phi_2|^2 + \frac{3}{2}\Gamma(|\phi_1|^2+|\phi_2|^2)^{1/2}|\phi_1|^2 + \Gamma(|\phi_1|^2+|\phi_2|^2)^{3/2} + V - \mu\right],$$

$$A_{12} = g\phi_1^2 + \frac{3}{2}\Gamma(|\phi_1|^2+|\phi_2|^2)^{1/2}\phi_1^2,$$

$$A_{13} = \frac{3}{2}\Gamma(|\phi_1|^2+|\phi_2|^2)^{1/2}\phi_1\phi_2^* - (g+\delta g)\phi_1\phi_2^*,$$

$$A_{14} = \frac{3}{2}\Gamma(|\phi_1|^2+|\phi_2|^2)^{1/2}\phi_1\phi_2 - (g+\delta g)\phi_1\phi_2, \tag{A1}$$

$$A_{21} = -g\phi_1^{*2} - \frac{3}{2}\Gamma(|\phi_1|^2+|\phi_2|^2)^{1/2}\phi_1^{*2},$$

$$A_{22} = \frac{1}{2}\left[\frac{d}{rdr} + \frac{d^2}{dr^2} - \frac{(S-m)^2}{r^2}\right] + (g+\delta g)|\phi_2|^2 - 2g|\phi_1|^2 - \frac{3}{2}\Gamma(|\phi_1|^2+|\phi_2|^2)^{1/2}|\phi_1|^2 - \Gamma(|\phi_1|^2+|\phi_2|^2)^{3/2} - V + \mu,$$

$$A_{23} = (g+\delta g)\phi_1^*\phi_2^* - \frac{3}{2}\Gamma(|\phi_1|^2+|\phi_2|^2)^{1/2}\phi_1^*\phi_2^*,$$

$$A_{24} = (g+\delta g)\phi_1^*\phi_2 - \frac{3}{2}\Gamma(|\phi_1|^2+|\phi_2|^2)^{1/2}\phi_1^*\phi_2, \tag{A2}$$

$$A_{31} = \frac{3}{2}\Gamma(|\phi_2|^2+|\phi_1|^2)^{1/2}\phi_2\phi_1^* - (g+\delta g)\phi_2\phi_1^*,$$

$$A_{32} = \frac{3}{2}\Gamma(|\phi_2|^2+|\phi_1|^2)^{1/2}\phi_2\phi_1 - (g+\delta g)\phi_2\phi_1,$$

$$A_{33} = -\frac{1}{2}\left[\frac{d}{rdr} + \frac{d^2}{dr^2} - \frac{(-S+m)^2}{r^2}\right] + 2g|\phi_2|^2 - (g+\delta g)|\phi_1|^2 + \frac{3}{2}\Gamma(|\phi_2|^2+|\phi_1|^2)^{1/2}|\phi_2|^2 + \Gamma(|\phi_2|^2+|\phi_1|^2)^{3/2} + V - \mu,$$

$$A_{34} = g\phi_2^2 + \frac{3}{2}\Gamma(|\phi_2|^2+|\phi_1|^2)^{1/2}\phi_2^2, \tag{A3}$$

$$A_{41} = (g + \delta g)\phi_1^* \phi_2^* - \frac{3}{2}\Gamma(|\phi_1|^2 + |\phi_2|^2)^{1/2}\phi_1^*\phi_2^*,$$

$$A_{42} = (g + \delta g)\phi_2^* \phi_1 - \frac{3}{2}\Gamma(|\phi_1|^2 + |\phi_2|^2)^{1/2}\phi_2^*\phi_1,$$

$$A_{43} = -g\phi_2^{*2} - \frac{3}{2}\Gamma(|\phi_2|^2 + |\phi_1|^2)^{1/2}\phi_2^{*2},$$

$$A_{44} = \frac{1}{2}\left[\frac{d}{rdr} + \frac{d^2}{dr^2} - \frac{(-S-m)^2}{r^2}\right] + (g + \delta g)|\phi_1|^2 - 2g|\phi_2|^2 - \frac{3}{2}\Gamma(|\phi_2|^2 + |\phi_1|^2)^{1/2}|\phi_2|^2 - \Gamma(|\phi_2|^2 + |\phi_1|^2)^{3/2} - V + \mu.$$

$$(A4)$$

[1] Y. Xu, Y. P. Zhang, and B. Wu, Bright solitons in spin-orbit-coupled Bose-Einstein condensates, Phys. Rev. A **87**, 013614 (2013).

[2] Y. L. Zhang, C. Y. Jia, and Z. X. Liang, Dynamics of two dark Solitons in a polariton condensate, Chin. Phys. Lett. **39**, 020501 (2022).

[3] X. M. Zhang, Y. H. Qin, L. M. Ling, and L. C. Zhao, Inelastic interaction of double-valley dark solitons for the Hirota equation, Chin. Phys. Lett. **38**, 090201 (2021).

[4] S. Wang, Y. H. Liu, and T. F. Xu, Gap solitons of spin- orbit-coupled Bose-Einstein condensates in PT periodic potential, Chin. Phys. B **31**, 070306 (2022).

[5] Y. H. Qin, Y. Wu, L. C. Zhao, and Z. Y. Yang, Interference properties of two-component matter wave solitons, Chin. Phys. B **29**, 020303 (2020).

[6] L. X. Wang, C. Q. Dai, L. Wen, T. Liu, H. F. Jiang, H. Saito, S. G. Zhang, and X. F. Zhang, Dynamics of vortices followed by the collapse of ring dark solitons in a two-component Bose-Einstein condensate, Phys. Rev. A **97**, 063607 (2018).

[7] C. Chin, R. Grimm, P. Julienne, and E. Tiesinga, Feshbach resonances in ultracold gases, Rev. Mod. Phys. **82**, 1225 (2010).

[8] E. Shamriz, Z. P. Chen, and B. A. Malomed, Stabilization of one-dimensional Townes solitons by spin-orbit coupling in a dual-core system, Commun. Nonlinear Sci. Numer. Simulat. **91**, 105412 (2020).

[9] B. A. Malomed, D. Mihalache, F. Wise, and L. Torner, Spatiotemporal optical solitons, J. Opt. B **7**, R53 (2005).

[10] L. Bergé, Wave collapse in physics: Principles and applications to light and plasma waves, Phys. Rep. **303**, 259 (1998).

[11] B. A. Malomed, *Multidimensional Solitons* (American Institute of Physics Publishing, Melville, 2022).

[12] X. Liu, K. Beckwitt, and F. Wise, Two-dimensional optical spatiotemporal solitons in quadratic media, Phys. Rev. E **62**, 1328 (2000).

[13] D. Mihalache, D. Mazilu, L. C. Crasovan, B. A. Malomed, and F. Lederer, Three-dimensional spinning solitons in the cubic-quintic nonlinear medium, Phys. Rev. E **61**, 7142 (2000).

[14] Y. Y. Wang, L. Chen, C. Q. Dai, J. Zheng, and Y. Fan, Exact vector multipole and vortex solitons in the media with spatially modulated cubic-quintic nonlinearity, Nonlinear Dyn. **90**, 1269 (2017).

[15] Y. X. Chen, L. H. Zheng, and F. Q. Xu, Spatiotemporal vector and scalar solitons of the coupled nonlinear Schrödinger equation with spatially modulated cubic-quintic-septimal nonlinearities, Nonlinear Dyn. **93**, 2379 (2018).

[16] J. T. Li, Y. Zhu, J. Z. Han, W. Qin, C. Q. Dai, and S. H. Wang, Scalar and vector multipole and vortex solitons in the spatially modulated cubic-quintic nonlinear media, Nonlinear Dyn. **91**, 757 (2018).

[17] M. Segev, G. C. Valley, B. Crosignani, P. DiPorto, and A. Yariv, Steady-state spatial screening solitons in photorefractive materials with external applied field, Phys. Rev. Lett. **73**, 3211 (1994).

[18] M. Peccianti, K. A. Brzdakiewicz, and G. Assanto, Nonlocal spatial soliton interactions in nematic liquid crystals, Opt. Lett. **27**, 1460 (2022).

[19] P. Pedri and L. Santos, Two-dimensional bright solitons in dipolar Bose-Einstein condensates, Phys. Rev. Lett. **95**, 200404 (2005).

[20] I. Tikhonenkov, B. A. Malomed, and A. Vardi, Anisotropic solitons in dipolar Bose-Einstein condensates, Phys. Rev. Lett. **100**, 090406 (2008).

[21] J. S. Huang, X. D. Jiang, H. Y. Chen, Z. W. Fan, W. Pang, and Y. Y. Li, Quadrupolar matter-wave soliton in two-dimensional free space, Front. Phys. **10**, 100507 (2015).

[22] F. Maucher, N. Henkel, M. Saffman, W. Królikowski, S. Skupin, and T. Pohl, Rydberg-induced solitons: Three-dimensional self-trapping of matter waves, Phys. Rev. Lett. **106**, 170401 (2011).

[23] T. D. Stanescu, B. Anderson, and V. Galitski, Spin-orbit coupled Bose-Einstein condensates, Phys. Rev. A **78**, 023616 (2008).

[24] Y. C. Zhang, Z. W. Zhou, B. A. Malomed, and H. Pu, Stable solitons in three dimensional free space without the ground state: Self-trapped Bose-Einstein condensates with spin-orbit coupling, Phys. Rev. Lett. **115**, 253902 (2015).

[25] H. Sakaguchi, B. Li, E. Y. Sherman, and B. A. Malomed, Composite solitons in two-dimensional spin-orbit coupled self-attractive Bose-Einstein condensates in free space, Rom. Rep. Phys. **70**, 502 (2018).

[26] B. Liu, R. X. Zhong, Z. P. Chen, X. Z. Qin, H. H. Zhong, Y. Y. Li, and B. A. Malomed, Holding and transferring matter-wave solitons against gravity by spin-orbit-coupling tweezers, New J. Phys. **22**, 043004 (2020).

[27] C. H. Tenorio, E. V. Vargas, V. N. Serkin, M. A. Granados, T. L. Belyaeva, R. P. Moreno, and L. M. Lara, Dynamics of

solitons in the model of nonlinear Schrödinger equation with an external harmonic potential: II. Dark solitons, Quantum Electron. **35**, 929 (2005).

[28] Z. H. Luo, Y. Liu, Y. Y. Li, J. Batle, and B. A. Malomed, Stability limits for modes held in alternating trapping-expulsive potentials, Phys. Rev. E **106**, 014201 (2022).

[29] M. R. Pathak and A. Nath, Dynamics of quantum droplets in an external harmonic confinement, Sci. Rep. **12**, 18248 (2022).

[30] M. Schmitt, M. Wenzel, F. Böttcher, I. Ferrier-Barbut, and T. Pfau, Self-bound droplets of a dilute magnetic quantum liquid, Nature (London) **539**, 259 (2016).

[31] L. Chomaz, S. Baier, D. Petter, M. J. Mark, F. Wächtler, L. Santos, and F. Ferlaino, Quantum-fluctuation-driven crossover from a dilute Bose-Einstein condensate to a macrodroplet in a dipolar quantum fluid, Phys. Rev. X **6**, 041039 (2016).

[32] C. R. Cabrera, L. Tanzi, J. Sanz, B. Naylor, P. Thomas, P. Cheiney, and L. Tarruell, Quantum liquid droplets in a mixture of Bose-Einstein condensates, Science **359**, 301 (2018).

[33] D. S. Petrov, Quantum mechanical stabilization of a collapsing Bose-Bose mixture, Phys. Rev. Lett. **115**, 155302 (2015).

[34] D. S. Petrov and G. E. Astrakharchik, Ultradilute low-dimensional liquids, Phys. Rev. Lett. **117**, 100401 (2016).

[35] T. D. Lee, K. S. Huang, and C. N. Yang, Eigenvalues and eigenfunctions of a Bose System of hard spheres and its low-temperature properties, Phys. Rev. **106**, 1135 (1957).

[36] M. Tylutki, G. E. Astrakharchik, B. A. Malomed, and D. S. Petrov, Collective excitations of a one-dimensional quantum droplet, Phys. Rev. A **101**, 051601(R) (2020).

[37] A. Boudjemâa, Fluctuations and quantum self-bound droplets in a dipolar Bose-Bose mixture, Phys. Rev. A **98**, 033612 (2018).

[38] A. Boudjemâa, Two-dimensional quantum droplets in dipolar Bose gases, New J. Phys. **21**, 093027 (2019).

[39] H. Hu and X. J. Liu, Microscopic derivation of the extended Gross-Pitaevskii equation for quantum droplets in binary Bose mixtures, Phys. Rev. A **102**, 043302 (2020).

[40] L. Parisi and S. Giorgini, Quantum droplets in one-dimensional Bose mixtures: A quantum Monte Carlo study, Phys. Rev. A **102**, 023318 (2020).

[41] R. N. Bisset, L. A. Peña Ardila, and L. Santos, Quantum droplets of dipolar mixtures, Phys. Rev. Lett. **126**, 025301 (2021).

[42] Y. V. Kartashov, B. A. Malomed, and L. Torner, Structured heterosymmetric quantum droplets, Phys. Rev. Res. **2**, 033522 (2020).

[43] S. R. Otajonov, E. N. Tsoy, and F. K. Abdullaev, Variational approximation for two-dimensional quantum droplets, Phys. Rev. E **102**, 062217 (2020).

[44] Z. H. Luo, W. Pang, B. Liu, Y. Y. Li, and B. A. Malomed, A new form of liquid matter: Quantum droplets, Front. Phys. **16**, 32201 (2021).

[45] B. Liu, H. F. Zhang, R. X. Zhong, X. L. Zhang, X. Z. Qin, C. Q. Huang, Y. Y. Li, and B. A. Malomed, Symmetry breaking of quantum droplets in a dual-core trap, Phys. Rev. A **99**, 053602 (2019).

[46] X. L. Cui, Spin-orbit-coupling-induced quantum droplet in ultracold Bose-Fermi mixtures, Phys. Rev. A **98**, 023630 (2018).

[47] Z. C. Guo, F. Jia, L. Li, Y. F. Ma, J. M. Hutson, X. L. Cui, and D. J. Wang, Lee-Huang-Yang effects in the ultracold mixture of ^{23}Na and ^{87}Rb with attractive interspecies interactions, Phys. Rev. Res. **3**, 033247 (2021).

[48] Y. Q. Wang, L. F. Guo, S. Yi, and T. Shi, Theory for self-bound states of dipolar Bose-Einstein condensates, Phys. Rev. Res. **2**, 043074 (2020).

[49] I. Ferrier-Barbut, M. Wenzel, F. Böttcher, T. Langen, M. Isoard, S. Stringari, and T. Pfau, Scissors mode of dipolar quantum droplets of dysprosium atoms, Phys. Rev. Lett. **120**, 160402 (2018).

[50] L. Dong and Y. V. Kartashov, Rotating multidimensional quantum qroplets, Phys. Rev. Lett. **126**, 244101 (2021).

[51] H. Huang, H. Wang, M. Chen, C. S. Lim, and K. Wong, Binary-vortex quantum droplets, Chaos Solitons Fractals **158**, 112079 (2022).

[52] M. Guo and T. Pfau, A new state of matter of quantum droplets, Front. Phys. **16**, 32202 (2021).

[53] Y. Y. Li, Z. H. Luo, Y. Liu, Z. P. Chen, C. Q. Huang, S. H. Fu, H. S. Tan, and B. A. Malomed, Two-dimensional solitons and quantum droplets supported by competing self- and cross-interactions in spin-orbit-coupled condensates, New J. Phys. **19**, 113043 (2017).

[54] B. A. Malomed, The family of quantum droplets keeps expanding, Front. Phys. **16**, 22504 (2021).

[55] S. L. Xu, Y. B. Lei, J. T. Du, Y. Zhao, R. Hua, and J. H. Zeng, Three-dimensional quantum droplets in spin-orbit-coupled Bose-Einstein condensates, Chaos Solitons Fractals **164**, 112665 (2022).

[56] Z. Zhou, Y. Shi, F. Ye, H. Chen, S. Tang, H. Deng, and H. Zhong, Self-bound states induced by the Lee-Huang-Yang effect in non-PT-symmetric complex potentials, Nonlinear Dyn. **110**, 3769 (2022).

[57] Z. Zhou, Y. M. Shi, S. Q. Tang, H. M. Deng, H. B. Wang, X. Y. He, and H. H. Zhong, Controllable dissipative quantum droplets in one-dimensional optical lattices, Chaos Solitons Fractals **150**, 111193 (2021).

[58] Y. M. Hu, Y. F. Fei, X. L. Chen, and Y. B. Zhang, Collisional dynamics of symmetric two-dimensional quantum droplets, Front. Phys. **17**, 61505 (2022).

[59] Y. V. Kartashov, V. M. Lashkin, M. Modugno, and L. Torner, Spinor-induced instability of kinks, holes and quantum droplets, New J. Phys. **24**, 073012 (2022).

[60] P. Zin, M. Pylak, and M. Gajda, Zero-energy modes of two-component Bose-Bose droplets, New J. Phys. **23**, 033022 (2021).

[61] V. Cikojević, L. V. Markić, and J. Boronat, Finite-range effects in ultradilute quantum drops, New J. Phys. **22**, 053045 (2020).

[62] A. Cidrim, L. Salasnich, and T. Macrí, Soliton trains after interaction quenches in Bose mixtures, New J. Phys. **23**, 023022 (2021).

[63] T. Karpiuk, M. Gajda, and M. Brewczyk, Bistability of Bose-Fermi mixtures, New J. Phys. **22**, 103025 (2020).

[64] F. Zhang and L. Yin, Phonon stability of quantum droplets in dipolar Bose gases, Chin. Phys. Lett. **39**, 060301 (2022).

[65] J. B. Wang, J. S. Pan, X. L. Cui, and W. Yi, Quantum droplets in a mixture of Bose-Fermi superfluids, Chin. Phys. Lett. **37**, 076701 (2020).

[66] J. Wang, X. J. Liu, and H. Hu, Ultradilute self-bound quantum droplets in Bose-Bose mixtures at finite temperature, Chin. Phys. B **30**, 010306 (2021).

[67] G. Ferioli, G. Semeghini, L. Masi, G. Giusti, G. Modugno, M. Inguscio, A. Gallemí, A. Recati, and M. Fattori, Collisions of self-bound quantum qroplets, Phys. Rev. Lett. **122**, 090401 (2019).

[68] G. Li, X. Jiang, B. Liu, Z. Chen, B. A. Malomed, and Y. Li, Two-dimensional anisotropic vortex quantum droplets in dipolar Bose-Einstein condensates, Front. Phys. **19**, 22202 (2024).

[69] A. W. Yang, G. L. Li, X. D. Jiang, Z. W. Fan, Z. P. Chen, B. Liu, and Y. Y. Li, Two-dimensional quantum droplets in binary dipolar Bose-Bose mixture, Photonics **10**, 405 (2023).

[70] Y. Y. Li, Z. P. Chen, Z. H. Luo, C. Q. Huang, H. S. Tan, W. Pang, and B. A. Malomed, Two-dimensional vortex quantum droplets, Phys. Rev. A **98**, 063602 (2018).

[71] Y. V. Kartashov, B. A. Malomed, L. Tarruell, and L. Torner, Three-dimensional droplets of swirling superfluids, Phys. Rev. A **98**, 013612 (2018).

[72] X. L. Zhang, X. X. Xu, Y. Y. Zheng, Z. P. Chen, B. Liu, C. Q. Huang, B. A. Malomed, and Y. Y. Li, Semidiscrete quantum droplets and vortices, Phys. Rev. Lett. **123**, 133901 (2019).

[73] Z. Zhou, X. Yu, Y. Zou, and H. H. Zhong, Dynamics of quantum droplets in a one-dimensional optical lattice, Commun. Nonlinear Sci. Numer. Simulat. **78**, 104881 (2019).

[74] F. Y. Zhao, Z. T. Yan, X. Y. Cai, C. L. Li, G. L. Chen, H. X. He, B. Liu, and Y. Y. Li, Discrete quantum droplets in one-dimensional optical lattices, Chaos Solitons Fractals **152**, 111313 (2021).

[75] L. W. Dong, W. Qi, P. Peng, L. X. Wang, H. Zhou, and C. M. Huang, Multi-stable quantum droplets in optical lattices, Nonlinear Dyn. **102**, 303 (2020).

[76] O. Morsch and M. Oberthaler, Dynamics of Bose-Einstein condensates in optical lattices, Rev. Mod. Phys. **78**, 179 (2006).

[77] Y. K. Liu and S. J. Yang, Three-dimensional solitons in two-component Bose-Einstein condensates, Chin. Phys. B **23**, 110308 (2014).

[78] Y. Y. Zheng, S. T. Chen, Z. P. Huang, S. X. Dai, B. Liu, Y. Y. Li, and S. R. Wang, Quantum droplets in two-dimensional optical lattices, Front. Phys. **16**, 22501 (2021).

[79] R. S. Yang and J. H. Yang, Effect of interaction strength on gap solitons of Bose-Einstein condensates in optical lattices, Chin. Phys. B **17**, 1189 (2008).

[80] Q. B. Wang, H. Yang, N. Su, and L. H. Wen, Ground-state phases and spin textures of spin-orbit-coupled dipolar Bose-Einstein condensates in a rotating toroidal trap, Chin. Phys. B **29**, 116701 (2020).

[81] Q. H. Cao and C. Q. Dai, Symmetric and anti-symmetric solitons of the fractional second- and third-order nonlinear Schrödinger equation, Chin. Phys. Lett. **38**, 090501 (2021).

[82] B. B. Li, Y. Zhao, S. L. Xu, Q. Zhou, Q. D. Fu, F. W. Ye, C. B. Hua, M. W. Chen, H. J. Hu, Q. Q. Zhou, and Z. C. Qiu, Two-dimensional gap solitons in parity-time symmetry Moiré optical lattices with Rydberg-Rydberg interaction, Chin. Phys. Lett. **40**, 044201 (2023).

[83] R. F. Zhang, X. F. Zhang, and L. Li, Exotic vortex structures of the dipolar Bose-Einstein condensates trapped in harmonic-like and toroidal potential, Phys. Lett. A **383**, 231 (2019).

[84] J. G. Wang, W. Wang, X. D. Bai, and S. J. Yang, Ring phases of spin-orbit coupled Bose-Einstein condensate in the radial optical lattices, Eur. Phys. J. Plus **134**, 27 (2019).

[85] X. F. Zhang, M. Kato, W. Han, S. G. Zhang, and H. Saito, Spin-orbit-coupled Bose-Einstein condensates held under a toroidal trap, Phys. Rev. A **95**, 033620 (2017).

[86] M. Brtka, A. Gammal, and B. A. Malomed, Hidden vorticity in binary Bose-Einstein condensates, Phys. Rev. A **82**, 053610 (2010).

[87] L. H. Wen, H. W. Xiong, and B. Wu, Hidden vortices in a Bose-Einstein condensate in a rotating double-well potential, Phys. Rev. A **82**, 053627 (2010).

[88] S. Subramaniyan, Vortex formation and hidden vortices in dipolar Bose-Einstein condensates, Phys. Lett. A **381**, 3062 (2017).

[89] C. Q. Huang, L. Lyu, H. Huang, Z. P. Chen, S. H. Fu, H. S. Tan, B. A. Malomed, and Y. Y. Li, Dipolar bright solitons and solitary vortices in a radial lattice, Phys. Rev. A **96**, 053617 (2017).

[90] B. Liu, Y. X. Chen, A. W. Yang, X. Y. Cai, Y. Liu, Z. H. Luo, X. Z. Qin, X. D. Jiang, Y. Y. Li, and B. A. Malomed, Vortex-ring quantum droplets in a radially-periodic potential, New J. Phys. **24**, 123026 (2022).

[91] G. Semeghini, G. Ferioli, L. Masi, C. Mazzinghi, L. Wolswijk, F. Minardi, M. Modugno, G. Modugno, M. Inguscio, and M. Fattori, Self-bound quantum droplets of atomic mixtures in free space, Phys. Rev. Lett. **120**, 235301 (2018).

[92] Z. D. Lin, X. X. Xu, Z. K. Chen, Z. T. Yan, Z. J. Mai, and B. Liu, Two-dimensional vortex quantum droplets get thick, Commun. Nonlinear Sci. Numer. Simulat. **93**, 105536 (2021).

[93] C. J. Pethick and H. Smith, *Bose-Einstein Condensation in Dilute Gases* (Cambridge University Press, Cambridge, 2008).

[94] B. Baizakov, B. A. Malomed, and M. Salerno, Matter-wave solitons in radially periodic potentials, Phys. Rev. E **74**, 066615 (2006).

[95] N. Gong, F. Y. Xu, J. Y. Yang, Y. L. Shi, Y. X. Qian, and Z. J. Ren, Generation of diffraction-free petallike beams based on stationary phase principle, Results Phys. **39**, 105698 (2022).

[96] L. M. Chiofalo, S. Succi, and P. M. Tosi, Ground state of trapped interacting Bose-Einstein condensates by an explicit imaginary-time algorithm, Phys. Rev. E **62**, 7438 (2000).

[97] J. K. Yang and T. I. Lakoba, Accelerated imaginary-time evolution methods for the computation of solitary waves, Stud. Appl. Math. **120**, 265 (2008).

[98] G. P. Agrawal, *Nonlinear Fiber Optics* (Academic Press, Amsterdam, 2013).

[99] N. G. Vakhitov and A. A. Kolokolov, Stationary solutions of the wave equation in media with nonlinearity saturation, Radiophys. Quantum Electron. **16**, 783 (1973).

[100] H. Sakaguchi and B. A. Malomed, Solitons in combined linear and nonlinear lattice potentials, Phys. Rev. A **81**, 013624 (2010).

[101] B. N. Aleksić, N. B. Aleksić, V. Skarka, and M. Beli ć, Stability and nesting of dissipative vortex solitons with high vorticity, Phys. Rev. A **91**, 043832 (2015).